

MAM4001W Project Thesis:
Chaotic Diffusion in Disordered Nonlinear Lattices

Jean-Jacq du Plessis*

University of Cape Town

16 September 2019


Abstract

We study the chaoticity and the diffusion of energy in one-dimensional disordered Klein-Gordon (KG) lattices. Building on the research of [B. Senyange *et al.*, *Phys. Rev. E*, 98:052229, 2019], we explore the effect of varying the disorder radius Δ on the chaoticity and diffusion of energy through the lattice from a single-site excitation. Computing the normal modes of the linearised KG model, we find that normal mode distributions have a greater spread in more ordered lattices. This suggests that energy diffuses faster through the nonlinear KG lattice when decreasing Δ . Computing the evolution of the KG system up to 10^7 (dimensionless) time units for various values of Δ , we find that the second moment m and participation number P of the wave packet evolve according to the power laws $m \propto t^{\alpha_m}$ and $P \propto t^{\alpha_P}$, respectively. While the constant of proportionality in each case is found to increase when decreasing Δ , no relationship between Δ and either of the values α_m, α_P is conclusively determined. We also find that the finite time maximum Lyapunov exponent (a commonly used chaos indicator) obeys a power law $\Lambda \propto t^{\alpha_\Lambda}$, and furthermore that α_Λ decreases with decreasing Δ , suggesting that more ordered KG lattices are less chaotic.

*Supervised by Associate Professor Haris Skokos.

Plagiarism Declaration

1. I know that plagiarism is a serious form of academic dishonesty.
2. I have read the UCT document [Avoiding Plagiarism: A guide for students](#), am familiar with its contents and have avoided all forms of plagiarism mentioned there.
3. Where I have used the words of others, I have indicated this by the use of quotation marks.
4. I have referenced all quotations and properly acknowledged other ideas borrowed from others.
5. I have not and shall not allow others to plagiarise my work.
6. I declare that this is my own work.

Signature: 

Acknowledgements

I would like to thank my project supervisor, Professor Haris Skokos, for his constant guidance and feedback on my progress throughout the year. I am also grateful to Bob Senyange for taking me under his wing and for answering my many questions. Finally, I would like to thank the other members of the Nonlinear Dynamics and Chaos Group at UCT for their useful advice and discussions, in particular: Many Manda, Malcolm Hillebrand, and Henok Moges. It has been a privilege to be a part of such an active, collaborative research group. Computations for this project were performed using facilities provided by the University of Cape Town's ICTS High Performance Computing team.

Contents

Plagiarism Declaration	1
Acknowledgements	1
1 Introduction	3
1.1 A Simple Lattice Model	3
1.2 Autonomous Hamiltonian Systems	3
1.3 Chaos	4
2 Klein-Gordon Model	4
2.1 Definitions	4
2.2 Equations of Motion and Variational Equations	5
2.3 Measuring Chaoticity	6
2.4 Research on Chaotic Diffusion	6
3 Computational Methods	7
3.1 Symplectic Integration	7
3.2 Optimising Python	9
3.3 Even Spacing in Log Scale	10
4 Linear System: Normal Mode Analysis	11
4.1 Linear KG Model	11
4.2 Normal Modes	12
4.3 Results	13
5 Nonlinear System: Wave Packet Evolution	15
5.1 Lattice Sizes	15
5.2 Parameters and Initial Conditions	15
5.3 Profile of Energy Distribution and DVD	17
5.4 Diffusion and Chaoticity Results	17
6 Discussion and Conclusion	21
References	22

1 Introduction

1.1 A Simple Lattice Model

Imagine a set of N particles, each labelled by an index $i \in \{1, 2, \dots, N\}$. Furthermore, let each particle be in its own attractive potential well V_i . What we have described is a system of N independent oscillators. Now consider the situation where we line these particles up according to their indices and connect each pair of neighbouring particles with a spring to form a one-dimensional (1D) chain or lattice. Finally, we attach each of the sites at the endpoints of the lattice (site 1 and site N) to an immovable wall. This setup is depicted in Figure 1.

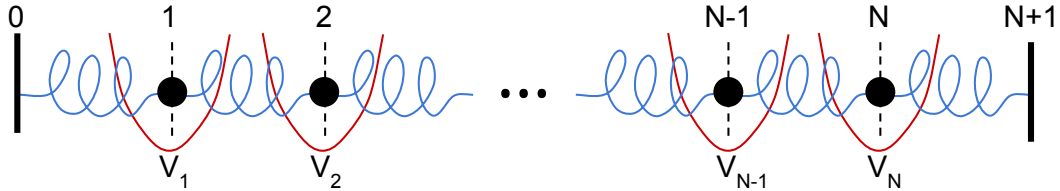


Figure 1: Diagram of a 1D lattice of oscillators, each with an on-site potential V_i (in red), coupled to its nearest neighbours via springs (in blue). Sites 0 and $N + 1$ are in fact immovable walls which are coupled to the endpoints of the lattice.

If the on-site potentials V_i and coupling spring potentials are of a certain form, then such a physical system may be described mathematically by a so-called Klein-Gordon (KG) lattice model with fixed boundary conditions (see Section 2 for more details). While this system of particles, potentials, and springs might seem contrived, such lattice models can be applied to simple molecular crystal structures including H_2 , N_2 , O_2 and NO [1, p. 77]. Since the potentials V_i need not be the same, such a disordered lattice may also be used to model the inhomogeneity of molecular bonds and metals which contain impurities or irregularities in their structure [2].

In this thesis, we are particularly interested in a class of 1D KG lattices which will be defined in Section 2.1. These involve quartic on-site potentials V_i with random variations for each site, producing a disordered nonlinear lattice. By giving energy to a single site in the middle of the lattice, we look at how energy diffuses through such a lattice over time in Section 5, as well as how chaotic the system is. In particular, we do this while varying the amount of disorder in the lattice to see what effect this might have. More fundamentally, we study this effect on a linear version of the lattice in Section 4 to understand the behaviour of normal modes and how they apply to the nonlinear KG lattice.

Before properly defining the KG model and discussing its properties, however, we must first introduce the necessary tools for the task.

1.2 Autonomous Hamiltonian Systems

The KG model which we will study describes a special type of continuous dynamical system, known as an autonomous Hamiltonian system. The state of an autonomous Hamiltonian system with N degrees of freedom is described by its generalised position $\vec{q} = (q_1, q_2, \dots, q_N)^T$ and its conjugate momentum $\vec{p} = (p_1, p_2, \dots, p_N)^T$, where each component q_i and p_i is a real variable, and the superscript T denotes the transpose. We represent this state by the vector $\vec{x} = (q_1, \dots, q_N, p_1, \dots, p_N)^T$ in a $2N$ -dimensional phase space [3, p. 68][4, p. 88]. Such a system has a Hamiltonian function

$H(\vec{q}, \vec{p})$, and the time evolution of the system is governed by Hamilton’s equations:

$$\frac{d\vec{q}}{dt} = \frac{\partial H}{\partial \vec{p}}, \quad \frac{d\vec{p}}{dt} = -\frac{\partial H}{\partial \vec{q}}. \quad (1)$$

For the class of dynamical systems which we will deal with, the Hamiltonian is given simply as the sum of all the kinetic and potential energy contributions to the total system.

1.3 Chaos

While chaos in dynamical systems can be defined in various ways, we will use a definition given by Devaney in [5, p. 50], which we restate here for convenience:

“Let V be a set. $f : V \rightarrow V$ is said to be chaotic in V if

1. f has sensitive dependence on initial conditions.
2. f is topologically transitive.
3. periodic points are dense in V .”

Condition 1 in this definition of chaos is a statement of the intrinsic unpredictability of chaotic systems. This is despite Condition 3, which requires that the system retains some form of regularity. Condition 2 further requires that a chaotic system cannot be decomposed into multiple subsystems. For further discussion, as well as mathematical definitions of each condition, refer to [5, pp. 49–50].

In practice, such complex definitions are often ignored and chaos is described only in terms of Condition 1 [3, pp. 65]. While sensitive dependence on initial conditions is often thought of as a fundamental property of chaos, it was shown that (in certain circumstances) this property can be derived from Conditions 2 and 3 in Devaney’s definition [6]. It is therefore not surprising that a universal definition of chaos has yet to be accepted. Nevertheless, when we discuss how to quantify the chaoticity of dynamical systems in Section 2.3, we will also focus our attention on this property of sensitive dependence on initial conditions.

2 Klein-Gordon Model

2.1 Definitions

Of interest to us is the 1D disordered quartic KG model studied (for example) in [7]. This lattice model has the Hamiltonian

$$H(\vec{q}, \vec{p}) = \sum_{i=0}^N \left[\frac{p_i^2}{2} + \frac{\epsilon_i}{2} q_i^2 + \frac{q_i^4}{4} + \frac{1}{2W} (q_{i+1} - q_i)^2 \right], \quad (2)$$

where q_i is the displacement from equilibrium of the i^{th} lattice site and p_i is its momentum conjugate, W is the disorder strength, and N is the number of coupled oscillators. Each ϵ_i is a disorder parameter chosen uniformly at random from the interval $[1 - \Delta, 1 + \Delta]$, where $\Delta \geq 0$ defines the disorder radius. For this model, we use the fixed boundary conditions $q_0 = q_{N+1} = p_0 = p_{N+1} = 0$, analogous to the fixed walls in Figure 1.

Inside the summation of equation (2), notice that the first term is the kinetic energy of a particular lattice site, the second and third terms form the on-site potential, and the last term is the coupling potential between neighbouring oscillators. Therefore, this model represents a specific case of the physical system depicted earlier in Figure 1.

We define the normalised energy distribution ξ_i for the i^{th} lattice site as the energy of that lattice site divided by the total energy H of the lattice. For the KG lattice, this is given by [7]

$$\xi_i = \frac{1}{H} \begin{cases} \frac{p_1^2}{2} + \frac{\epsilon_1}{2} q_1^2 + \frac{q_1^4}{4} + \frac{1}{4W} (q_2 - q_1)^2 + \frac{1}{2W} q_1^2, & \text{for } i = 1 \\ \frac{p_i^2}{2} + \frac{\epsilon_i}{2} q_i^2 + \frac{q_i^4}{4} + \frac{1}{4W} (q_{i+1} - q_i)^2 + \frac{1}{4W} (q_i - q_{i-1})^2, & \text{for } 1 < i < N \\ \frac{p_N^2}{2} + \frac{\epsilon_N}{2} q_N^2 + \frac{q_N^4}{4} + \frac{1}{4W} (q_N - q_{N-1})^2 + \frac{1}{2W} q_N^2, & \text{for } i = N. \end{cases} \quad (3)$$

As seen in this definition, we have made the choice that the energy belonging to a site is comprised of the site's kinetic energy, its on-site potential, and half of its coupling potential with each neighbour. The endpoints of the lattice (sites 1 and N) are an exception, as they contain all the energy in the coupling potential with their adjacent boundaries.

Now ξ_i is a normalised distribution with respect to the lattice in the sense that $\sum_{i=1}^N \xi_i = 1$. Therefore, we can define the mean $\bar{i} = \sum_{i=1}^N i \xi_i$ of the energy distribution as we would with a statistical distribution. From this, we define quantities which describe the spread of energy in the lattice, namely the second moment m and the participation number P (see e.g. [7]):

$$m = \sum_{i=1}^N (i - \bar{i})^2 \xi_i, \quad P = \left(\sum_{i=1}^N \xi_i^2 \right)^{-1}. \quad (4)$$

The second moment m is in fact the statistical variance of the distribution. The less well-known quantity P is a number which varies between 1 when all energy is contained within a single lattice site and N when all lattice sites share the energy equally. Hence, the participation number is in some sense an indicator of how many lattice sites ‘‘participate’’ in the sharing of energy, as the name would suggest.

2.2 Equations of Motion and Variational Equations

Calculating Hamilton's equations (1) from the KG Hamiltonian (2) yields the equations of motion:

$$\begin{aligned} \frac{dq_i}{dt} &= p_i \\ \frac{dp_i}{dt} &= - \left[\epsilon_i q_i + q_i^3 + \frac{1}{W} (2q_i - q_{i-1} - q_{i+1}) \right], \end{aligned} \quad (5)$$

where $1 \leq i \leq N$.

Consider now a point $\vec{x} = (\vec{q}, \vec{p})^T$ on some orbit in the system's phase space, and consider a small deviation from this orbit, $\delta\vec{x} = (\delta\vec{q}, \delta\vec{p})^T$. The evolution of this deviation vector over time is given by the so-called variational equations, defined (for example) in [3, pp. 69–70]. Calculating the variational equations from the KG Hamiltonian results in

$$\begin{aligned} \frac{d(\delta q_i)}{dt} &= \delta p_i, \quad \text{for } 1 \leq i \leq N \\ \frac{d(\delta p_i)}{dt} &= - \begin{cases} (\epsilon_1 + 3q_1^2)\delta q_1 + \frac{1}{W}(2\delta q_1 - \delta q_2), & \text{for } i = 1 \\ (\epsilon_i + 3q_i^2)\delta q_i + \frac{1}{W}(2\delta q_i - \delta q_{i-1} - \delta q_{i+1}), & \text{for } 1 < i < N \\ (\epsilon_N + 3q_N^2)\delta q_N + \frac{1}{W}(2\delta q_N - \delta q_{N-1}), & \text{for } i = N. \end{cases} \end{aligned} \quad (6)$$

These results for the equations of motion and the variational equations can also be found in [8], where the same KG Hamiltonian is studied.

2.3 Measuring Chaoticity

In order to quantify how chaotic a dynamical system is, we use the fact that chaotic systems exhibit sensitive dependence on initial conditions (recall Section 1.3). The maximum Lyapunov Exponent (MLE) is defined as (see e.g. [3, pp. 92–93])

$$\Lambda = \lim_{t \rightarrow \infty} \Lambda(t) = \lim_{t \rightarrow \infty} \frac{1}{t} \ln \frac{\|\delta\vec{x}(t)\|}{\|\delta\vec{x}(0)\|}, \quad (7)$$

where $\Lambda(t)$ is the finite time MLE, $\delta\vec{x}(0)$ is a randomly chosen initial deviation vector from an orbit in the phase space, and $\delta\vec{x}(t)$ is the deviation vector at some later time t . Loosely speaking, the MLE for an orbit is the rate of exponential growth of infinitesimally small deviations from that orbit. For regular orbits whose deviation vectors grow at a polynomial rate, their finite time MLEs tend to zero according to the power law $\Lambda \propto t^{-1}$ (asymptotically). On the other hand, chaotic orbits have positive MLEs [3, p. 65] as a result of an exponential growth rate of deviation vectors. For the KG model, however, we will be interested in a regime of chaos called weak chaos [9][10] for which the finite time MLE also approaches zero, though at a slower rate than for regular orbits [7][11].

Using the deviation vector $\delta\vec{x}$ evaluated at some point in time, we can determine how much each site of the KG lattice contributes to the overall deviation by computing the so-called normalised deviation vector distribution (DVD) [11]:

$$\xi_i^D = \frac{\delta q_i^2 + \delta p_i^2}{\sum_{j=1}^N (\delta q_j^2 + \delta p_j^2)}, \quad (8)$$

where $1 \leq i \leq N$. Since the largest components of $\delta\vec{x}$ are the greatest contributors to the MLE, the DVD is a good indicator of which regions of the lattice are the most chaotic at any moment in time.

2.4 Research on Chaotic Diffusion

In [7][9][10], the diffusion of energy through a KG lattice was studied. In particular, a single-site excitation was used, where only the middle site of the lattice was given energy initially (purely in the form of kinetic energy). Using $W = 4$, $\Delta = 0.5$, and a total energy of $H = 0.4$, it was shown that such a KG lattice exhibits weak chaos. Furthermore, by computing the state of the system up to a final time of 10^8 time units, they showed that the second moment, participation number, and MLE obeyed the following power laws (asymptotically): $m \propto t^{1/3}$, $P \propto t^{1/6}$, $\Lambda \propto t^{-1/4}$.

We wish to build on the research in [7] by exploring how changing the value of the disorder radius Δ affects the behaviour of m , P , and Λ . In particular, we decrease the value of Δ from 0.5 in order to approach the dynamics of an ordered lattice, i.e. $\Delta = 0$. As we will see, however, computing the state of the KG lattice for times up to 10^7 units with a small Δ value requires a large lattice size N , since we must avoid energy reaching the boundaries of the lattice. This in turn requires a long time to compute. The following values for the disorder radius are studied in this thesis: $\Delta \in \{0.08, 0.09, 0.1, 0.15, 0.2, 0.3, 0.4, 0.5\}$, where smaller values of Δ are not used due to the long computation time needed.

3 Computational Methods

3.1 Symplectic Integration

We now address issues of numerical integration of autonomous Hamiltonian systems. To quantify the numerical error of such integration schemes, we define the absolute relative energy error E_r as

$$E_r = \left| \frac{H - H_0}{H_0} \right|, \quad (9)$$

where H_0 is the initial value of the Hamiltonian and H is the computed value of the Hamiltonian at some later time. Now for autonomous Hamiltonian systems, the value of H should remain constant over time [12, p.67], thus any non-zero value of E_r must be a result of numerical error in the computation. E_r can therefore be used as an indicator of the accuracy of such computations.

Many general-purpose numerical integration schemes (e.g. Runge-Kutta 4th order [13, p.288]) yield values of E_r which grow unbounded in time, making them unsuitable for solving autonomous Hamiltonian systems over long periods of time. We therefore use symplectic integrators (SIs) in our study, which are numerical schemes for solving autonomous Hamiltonian systems with the property that they keep the value of E_r bounded [14], ensuring the integrity of the results.

We now demonstrate the application of a particular symplectic integration scheme to the KG model, namely the ABA864 [15] scheme. From the KG Hamiltonian given in (2), we see that it can easily be split into two parts, A and B , such that $H = A + B$. We use the following splitting of H :

$$\begin{aligned} A(\vec{p}) &= \sum_{i=0}^N \frac{p_i^2}{2}, \\ B(\vec{q}) &= \sum_{i=0}^N \left[\frac{\epsilon_i}{2} q_i^2 + \frac{q_i^4}{4} + \frac{1}{2W} (q_{i+1} - q_i)^2 \right]. \end{aligned} \quad (10)$$

Notice that A is only a function of \vec{p} , while B is only a function of \vec{q} . If we treat A as a Hamiltonian by itself, we can calculate the equations of motion and the variational equations for A , which together form the following system:

$$\begin{aligned} \frac{dq_i}{dt} &= p_i \\ \frac{dp_i}{dt} &= 0 \\ \frac{d(\delta q_i)}{dt} &= \delta p_i \\ \frac{d(\delta p_i)}{dt} &= 0, \end{aligned} \quad (11)$$

where $1 \leq i \leq N$. This system may be written simply as $d\vec{u}/dt = L_{AV}\vec{u}$, where $\vec{u} = (\vec{q}, \vec{p}, \vec{\delta q}, \vec{\delta p})^T$ and L_{AV} is the operator on the combined system. The solution of this equation follows readily: $\vec{u}(t) = e^{tL_{AV}}\vec{u}(0)$. Defining $\vec{u}' = \vec{u}(\tau)$ for some time step τ , we can write this solution in full:

$$\begin{aligned} q'_i &= q_i + \tau p_i \\ p'_i &= p_i \\ \delta q'_i &= \delta q_i + \tau \delta p_i \\ \delta p'_i &= \delta p_i, \end{aligned} \quad (12)$$

where $1 \leq i \leq N$. Therefore, we have analytically solved the Hamiltonian system described by A .

By similarly treating B as a Hamiltonian, we get the following combined system of equations of motion and variational equations:

$$\begin{aligned}
\frac{dq_i}{dt} &= 0, & \text{for } 1 \leq i \leq N \\
\frac{dp_i}{dt} &= - \begin{cases} \epsilon_1 q_1 + q_1^3 + \frac{1}{W}(2q_1 - q_2), & \text{for } i = 1 \\ \epsilon_i q_i + q_i^3 + \frac{1}{W}(2q_i - q_{i-1} - q_{i+1}), & \text{for } 1 < i < N \\ \epsilon_N q_N + q_N^3 + \frac{1}{W}(2q_N - q_{N-1}), & \text{for } i = N \end{cases} \\
\frac{d(\delta q_i)}{dt} &= 0, & \text{for } 1 \leq i \leq N \\
\frac{d(\delta p_i)}{dt} &= - \begin{cases} (\epsilon_1 + 3q_1^2)\delta q_1 + \frac{1}{W}(2\delta q_1 - \delta q_2), & \text{for } i = 1 \\ (\epsilon_i + 3q_i^2)\delta q_i + \frac{1}{W}(2\delta q_i - \delta q_{i-1} - \delta q_{i+1}), & \text{for } 1 < i < N \\ (\epsilon_N + 3q_N^2)\delta q_N + \frac{1}{W}(2\delta q_N - \delta q_{N-1}), & \text{for } i = N, \end{cases}
\end{aligned} \tag{13}$$

which can be abbreviated as $d\vec{u}/dt = L_{BV}\vec{u}$. Defining $\vec{u}' = \vec{u}(\tau)$, we may similarly write the analytical solution $\vec{u}(t) = e^{tL_{BV}}\vec{u}(0)$ in full:

$$\begin{aligned}
q'_i &= q_i, & \text{for } 1 \leq i \leq N \\
p'_i &= p_i - \tau \begin{cases} \epsilon_1 q_1 + q_1^3 + \frac{1}{W}(2q_1 - q_2), & \text{for } i = 1 \\ \epsilon_i q_i + q_i^3 + \frac{1}{W}(2q_i - q_{i-1} - q_{i+1}), & \text{for } 1 < i < N \\ \epsilon_N q_N + q_N^3 + \frac{1}{W}(2q_N - q_{N-1}), & \text{for } i = N \end{cases} \\
\delta q'_i &= \delta q_i, & \text{for } 1 \leq i \leq N \\
\delta p'_i &= \delta p_i - \tau \begin{cases} (\epsilon_1 + 3q_1^2)\delta q_1 + \frac{1}{W}(2\delta q_1 - \delta q_2), & \text{for } i = 1 \\ (\epsilon_i + 3q_i^2)\delta q_i + \frac{1}{W}(2\delta q_i - \delta q_{i-1} - \delta q_{i+1}), & \text{for } 1 < i < N \\ (\epsilon_N + 3q_N^2)\delta q_N + \frac{1}{W}(2\delta q_N - \delta q_{N-1}), & \text{for } i = N. \end{cases}
\end{aligned} \tag{14}$$

These results for the two part splitting of the KG Hamiltonian into A and B can also be found in [8].

Using the so-called tangent map method [16], a symplectic integration scheme involving successive applications of the operators $e^{\tau L_{AV}}$ and $e^{\tau L_{BV}}$ can be used to numerically solve both Hamilton's equations and the variational equations together. The symplectic integrator $ABA864$ can be used to numerically integrate the KG system in this manner, and is defined as

$$\begin{aligned}
ABA864(\tau) &= e^{a_1\tau L_{AV}} e^{b_1\tau L_{BV}} e^{a_2\tau L_{AV}} e^{b_2\tau L_{BV}} e^{a_3\tau L_{AV}} e^{b_3\tau L_{BV}} e^{a_4\tau L_{AV}} \\
&\quad \times e^{b_4\tau L_{BV}} e^{a_4\tau L_{AV}} e^{b_3\tau L_{BV}} e^{a_3\tau L_{AV}} e^{b_2\tau L_{BV}} e^{a_2\tau L_{AV}} e^{b_1\tau L_{BV}} e^{a_1\tau L_{AV}}
\end{aligned} \tag{15}$$

where the coefficients a_i and b_i are given in [15], which we restate here:

$$\begin{aligned}
a_1 &= 0.0711334264982231177779387300061549964174 \\
a_2 &= 0.241153427956640098736487795326289649618 \\
a_3 &= 0.521411761772814789212136078067994229991 \\
a_4 &= -0.333698616227678005726562603400438876027 \\
b_1 &= 0.183083687472197221961703757166430291072 \\
b_2 &= 0.310782859898574869507522291054262796375 \\
b_3 &= -0.0265646185119588006972121379164987592663 \\
b_4 &= 0.0653961422823734184559721793911134363710.
\end{aligned} \tag{16}$$

This SI in particular was determined in [8] to be the most efficient SI for integrating the KG system when compared with numerous other established SIs. We therefore use *ABA864* exclusively in computations involving numerical integration which follow, as it is both an efficient scheme and its symplectic nature keeps the value of E_r appropriately bounded.

3.2 Optimising Python

All computations for this thesis were done using the Python 3.7 programming language [17]. As Python is an interpreted, general-purpose language, it suffers the fate of being slower at some numerical tasks than other languages like Fortran, which are better suited to such computations. In order to perform efficient computations, it was therefore necessary to optimise our Python codes in order to approach the speed of Fortran and similar languages. While many techniques were used to increase the speed of our codes, the two most effective ones were vectorisation and compilation. Only these will be discussed.

In order to numerically integrate the equations of motion and the variational equations, the symplectic integrator *ABA864* defined in equation (15) was implemented at each time step of the computation. As an example, here is a Python code snippet of the implementation we used:

```

1  import numpy
2  from numba import jit
3
4  @jit
5  def ABA864(dt, X):
6      X[0] = X[0] + X[1]*a1*dt
7      X[2] = X[2] + X[3]*a1*dt
8      X[1,1:-1] = X[1,1:-1] - (eps*X[0,1:-1] + X[0,1:-1]**3 + (2*X[0,1:-1] -
9      ↪ X[0,:-2] - X[0,2:])/W)*b1*dt
10     X[3,1:-1] = X[3,1:-1] - (eps*X[2,1:-1] + 3*X[2,1:-1]*X[0,1:-1]**2 +
11     ↪ (2*X[2,1:-1] - X[2,:-2] - X[2,2:])/W)*b1*dt
12     X[0] = X[0] + X[1]*a2*dt
13     X[2] = X[2] + X[3]*a2*dt
14     X[1,1:-1] = X[1,1:-1] - (eps*X[0,1:-1] + X[0,1:-1]**3 + (2*X[0,1:-1] -
15     ↪ X[0,:-2] - X[0,2:])/W)*b2*dt
16     X[3,1:-1] = X[3,1:-1] - (eps*X[2,1:-1] + 3*X[2,1:-1]*X[0,1:-1]**2 +
17     ↪ (2*X[2,1:-1] - X[2,:-2] - X[2,2:])/W)*b2*dt
18     ... # steps omitted for brevity
19     return X

```

The function `ABA864` defined in Line 5 takes the time step `dt` as input, as well as the array `X` which consists of the vectors \vec{q} , \vec{p} , $\delta\vec{q}$ and $\delta\vec{p}$, respectively.¹ In Lines 6–7 we apply $e^{a_1\tau L_{AV}}$ to the current state, in Lines 8–9 we apply $e^{b_1\tau L_{BV}}$ to the current state, in Lines 10–11 we apply $e^{a_2\tau L_{AV}}$ to the current state, and so on until all steps comprising `ABA864` have been performed, after which the final state `X` is returned in Line 15. Compare each of these steps to equations (12) and (14), and the overall function to (15). Note that `eps` is a vector containing the disorder parameters ϵ_i for each lattice site. The `ABA864` function is then repeated in a loop, propagating the state forward in time by `dt` in each step.

The first optimisation technique we applied in this code was that of vectorisation. Notice that each line of the `ABA864` function is a vector equation, and the only operations used are addition and multiplication of vectors (component-wise). The Python library which provides the array data structure and the appropriate methods for this purpose is called NumPy [18], imported in Line 1. One complication in the vectorisation process was the fact that (14) requires adding and subtracting different components of the same vector, e.g. $(2q_i - q_{i-1} - q_{i+1})$. This was coded in a vectorised way by simply slicing the appropriate vector in different ways and adding/subtracting the results, e.g. `(2*X[0,1:-1] - X[0, :-2] - X[0, 2:])`. By completely vectorising these steps (as in the code snippet) as opposed to computing each vector component separately using loops, the computation time required by our implementation of the `ABA864` integrator in Python was reduced by an order of magnitude.

Despite vectorising our Python code as far as possible, it was still found to take an order of magnitude longer to execute than comparable codes written in Fortran. The other main optimisation technique which was then used was the runtime compilation of the `ABA864` function. The library Numba is a just-in-time (JIT) compiler which translates Python functions into efficient machine code at runtime [19]. This compiler was used in the code snippet by importing `numba` in Line 2 and adding the decorator `@jit` in Line 4 before the `ABA864` function. After using this compiler, the time taken for our Python code to execute was found to be on the same order of magnitude as comparable code written in Fortran. It should be noted, however, that Numba incurs some time overhead, so its use is more appropriate for long computations because this overhead may actually slow down short computations.

3.3 Even Spacing in Log Scale

In order to easily discern power laws from the types of results we will deal with in later sections, it is often convenient to present data in logarithmic (log) scale. Saving only the relevant data in such a scale requires some additional code which we discuss here.

Consider the time interval $[10^0, 10^3]$ units with a time step of 1 unit. Imagine performing some computations and saving the results at each time step in this interval. In log scale (base 10), the points in time at which data are saved for such a system are plotted on a number line in Figure 2. Notice that in this scale the saved points in time become so dense near the end of the time line that they are indistinguishable from their neighbours.

These data can instead be represented more sensibly in log scale by storing values at, say, only 100 points in time during the computation.² We choose these 100 points to be evenly spaced in log scale, as opposed to evenly spaced in linear scale. Such an ideal spacing of these (approximately) 100 points is given in Figure 3. Notice that, in this case, as soon as the gap between consecutive

¹However, these vectors also contain components for the boundaries of the lattice, indexed as sites 0 and $N + 1$. This was only done for convenience when coding; these components are not important for the computation.

²We only use 100 points here for demonstration purposes. When we present computation results later, we use 1000 points for a higher resolution.

time steps becomes too small in log scale, these points in time are repeatedly skipped over until the next point in time is appropriately spaced (in log scale) from the previously saved point. Thus our set of saved points in Figure 3 is less dense and more evenly spaced than before. Another advantage of such a restriction is the reduced number of times at which certain computations are done, and hence this may speed up some codes significantly.

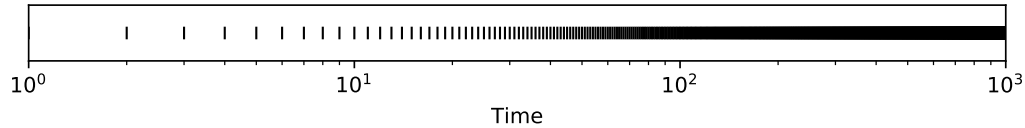


Figure 2: Number line (in log scale) of each time step over the interval $[10^0, 10^3]$.

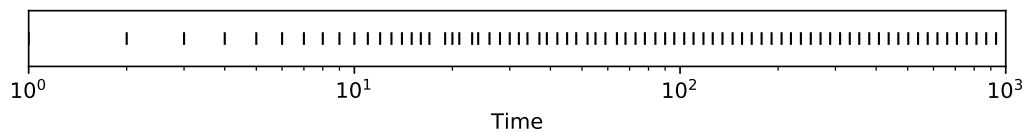


Figure 3: Number line of approximately 100 points in time spaced evenly in log scale over the interval $[10^0, 10^3]$.

How do we code the ideal spacing given in Figure 3? Since we are only interested in selecting 100 evenly spaced points in log scale from the interval $[10^0, 10^3]$, the ideal times t which we select would be when $\log_{10} t = 3k/100$ for any integer $k \in [0, 100]$. This would produce a perfectly even spacing in log scale by dividing the interval of length 3 (in log scale) into 100 equal sub-intervals. In practice, however, this equality would never be satisfied exactly, therefore we instead take note of when the value of $\log_{10} t$ changes from less than $3k/100$ to greater than $3k/100$. A Python code snippet of the algorithm described is given here:

```

1  from numpy import log10
2  k = 0
3  for t in range(1,10**3):
4      if log10(t) >= 3*k/100:
5          # do necessary computations here
6          while log10(t) >= 3*k/100:
7              k = k + 1

```

Once the condition $\log_{10}(t) \geq 3k/100$ in Line 4 is satisfied for some time t , we may perform all necessary computations and save relevant data at that point in time. In Lines 6–7, we increment k until $\log_{10}(t) \geq 3k/100$ is no longer true before increasing the time t and repeating the process.

4 Linear System: Normal Mode Analysis

4.1 Linear KG Model

Before explicitly computing the evolution of a wave packet through a KG lattice, we first examine a linear version of the KG model. By studying how normal modes are distributed in the linear lattice, we aim to understand and predict how energy diffuses in the (nonlinear) KG lattice.

We begin by linearising the KG lattice model. This is done by simply omitting the quartic potential terms in the KG Hamiltonian (2), since these are the terms of the Hamiltonian which produce the nonlinearity in the equations of motion. For small oscillations of the lattice sites, however, we can approximate the behaviour of the KG lattice by studying the linearised version which has the Hamiltonian

$$H(\vec{q}, \vec{p}) = \sum_{i=0}^N \left[\frac{p_i^2}{2} + \frac{\epsilon_i}{2} q_i^2 + \frac{1}{2W} (q_{i+1} - q_i)^2 \right]. \quad (17)$$

This lattice is the 1D disordered linear Klein-Gordon (LKG) model. Without the nonlinearity, note that the LKG lattice is nothing but a chain of disordered coupled harmonic oscillators, a system which we can solve explicitly.

4.2 Normal Modes

Using Hamilton's equations (1), the LKG Hamiltonian yields the following equations of motion:

$$\begin{aligned} \frac{dq_i}{dt} &= p_i \\ \frac{dp_i}{dt} &= - \left[\epsilon_i q_i + \frac{1}{W} (2q_i - q_{i-1} - q_{i+1}) \right] \end{aligned} \quad (18)$$

where $1 \leq i \leq N$. This can be reduced from a system of $2N$ first-order differential equations to N second-order differential equations,

$$\frac{d^2 q_i}{dt^2} = - \left[\epsilon_i q_i + \frac{1}{W} (2q_i - q_{i-1} - q_{i+1}) \right]. \quad (19)$$

The resulting linear system can be written simply as a vector equation,

$$\frac{d^2 \vec{q}}{dt^2} = \Omega \vec{q}, \quad (20)$$

where Ω is the tridiagonal matrix

$$\Omega = \begin{bmatrix} -\frac{2}{W} - \epsilon_1 & \frac{1}{W} & 0 & \cdots & 0 \\ \frac{1}{W} & -\frac{2}{W} - \epsilon_2 & \frac{1}{W} & \ddots & \vdots \\ 0 & \frac{1}{W} & -\frac{2}{W} - \epsilon_3 & \ddots & 0 \\ \vdots & \ddots & \ddots & \ddots & \frac{1}{W} \\ 0 & \cdots & 0 & \frac{1}{W} & -\frac{2}{W} - \epsilon_N \end{bmatrix}. \quad (21)$$

Now Ω has eigenvalues λ_k , as well as normalised eigenvectors \vec{v}_k which are the so-called normal modes of the LKG system [10]. Since Ω is Hermitian, its eigenvectors form a complete eigenbasis, and hence the solution of (20) can be written in the form $\vec{q} = \sum_k \hat{q}_k \vec{v}_k$, where \hat{q}_k are components of the solution in the eigenbasis. Since equation (20) reduces to $d^2 \hat{q}_k / dt^2 = \lambda_k \hat{q}_k$ in the eigenbasis, each \hat{q}_k has either a sinusoidal, linear, or exponential solution (depending on whether λ_k is negative, zero,

or positive). Despite the intrinsic randomness of the matrix Ω , we show in the following paragraph that each of its eigenvalues λ_k are negative in this case and hence each \hat{q}_k is sinusoidal.

Assume, to the contrary, that one of the eigenvalues λ_j of Ω is non-negative. Since we only use values of $\Delta < 1$, it follows that $0 < \epsilon_i < 2$, and hence all terms in the LKG Hamiltonian are non-negative. However, since \hat{q}_j corresponds to a non-negative eigenvalue λ_j , its solution will be either linear or exponential, and such terms would be present in linear combinations when converting this solution back into lattice coordinates. Such unbounded solutions would cause some terms in the LKG Hamiltonian to diverge over time, and hence the entire Hamiltonian would also diverge since it contains no negative terms to counter the divergence. This contradicts the fact that the Hamiltonian is conserved. Therefore, Ω only has negative eigenvalues.

4.3 Results

For an LKG lattice of size $N = 1001$ sites and disorder strength $W = 4$, we computed the eigenvalues and eigenvectors of Ω for each disorder radius $\Delta \in \{0.08, 0.09, 0.1, 0.15, 0.2, 0.3, 0.4, 0.5\}$. This was done using an algorithm designed for tridiagonal matrices [20]. Each eigenvector \vec{v}_k corresponds to a normal mode, and its components v_{ki} give the contributions of each lattice site to that normal mode. Since each \vec{v}_k is normalised, it follows that $\sum_i v_{ki}^2 = 1$. Therefore, we call the quantity v_{ki}^2 a normal mode distribution, since it describes the distribution of lattice sites participating in the k^{th} normal mode.

In the case of $\Delta = 0.5$, we plot each normal mode distribution v_{ki}^2 over the lattice in Figure 4 for a single disorder realisation of ϵ_i values. For clarity of demonstration, we only plot 30 random normal mode distributions, since all 1001 distributions would make the figure too dense to be useful. We see from Figure 4 that each normal mode is localised within the lattice, a phenomenon known as Anderson localisation [21].

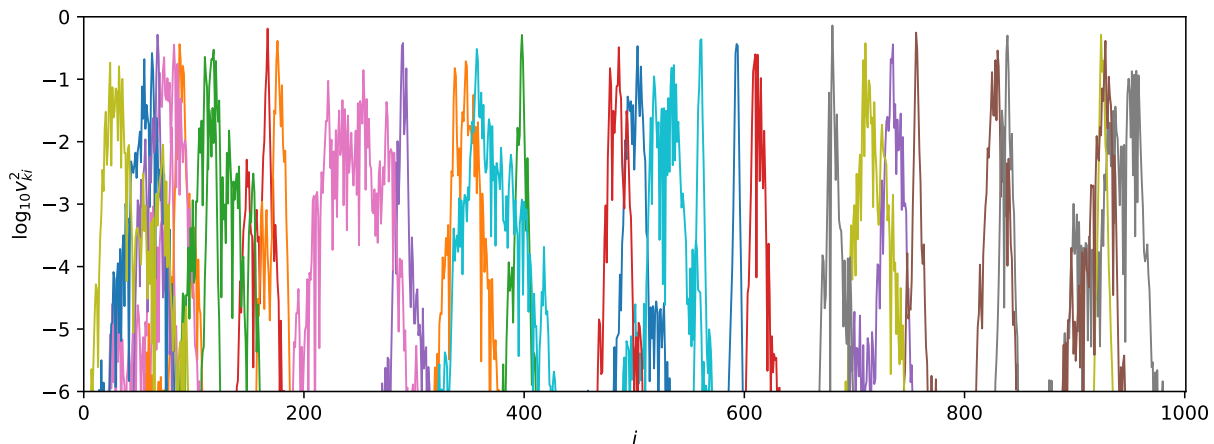


Figure 4: Plot of normal mode distributions v_{ki}^2 (in log scale) against lattice sites i for 30 normal modes. Due to limited choices, some distinct distributions share the same colour.

For each normal mode distribution v_{ki}^2 , we can compute its distribution mean \bar{i}_k , participation number P_k , and its second moment m_k . Note that the definitions of m_k and P_k are the same as in equations (4), except we replace the energy distribution ξ_i with v_{ki}^2 . In Figure 5(a) we plot the value of m_k for each normal mode distribution against its corresponding mean \bar{i}_k . This is done for each Δ value of interest, using a random disorder realisation in each case. From this figure we see

that normal modes centred around sites near the middle of the lattice tend to have larger values of m_k . This may be partially explained by the fact that normal mode distributions centred around sites near the tails of the lattice cannot have large spreads because of the nearby boundary. Centred near the middle of the lattice, however, the spread of each normal mode distribution does not have this constraint.

Figure 5(a) also indicates that m_k values tend to increase on average and have a greater spread as Δ decreases. To see this more clearly, we compute the mean \bar{m} of the second moment values m_k corresponding to each value of Δ . We also compute the spread of each set of m_k values using the standard deviation (SD). A plot of \bar{m} against Δ is given in Figure 5(b), where error bars indicate one SD from \bar{m} . For consistency and convenience, we use the same colour-code for points corresponding to the same Δ value in both Figures 5(a) and (b), and we will maintain this colour scheme in all figures which follow.

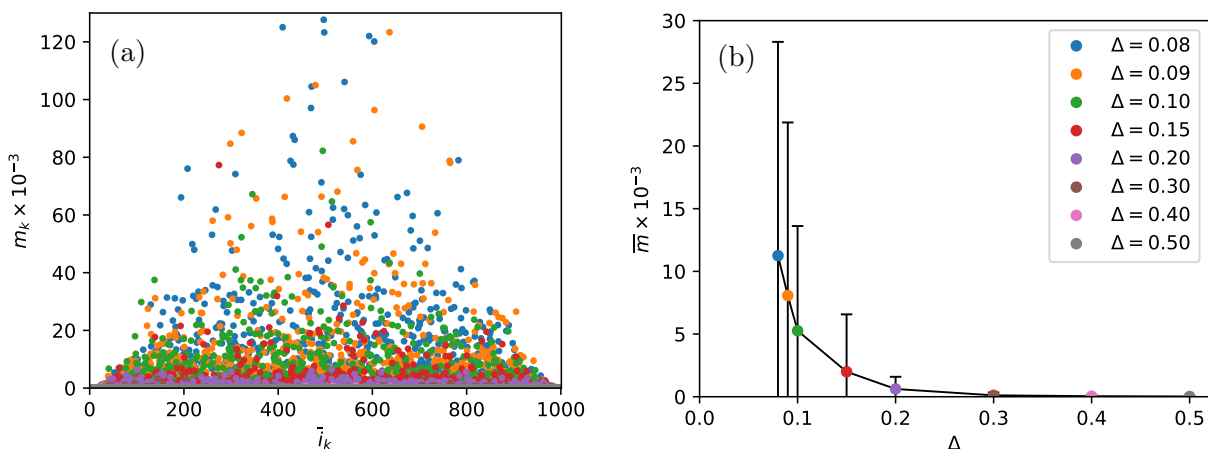


Figure 5: (a) Plot of second moment m_k of normal mode distribution v_{ki}^2 against the distribution mean \bar{i}_k , where each colour represents a value of Δ given in the legend of (b). (b) Plot of mean second moment \bar{m} against disorder radius Δ . Error bars indicate one SD from \bar{m} .

Similarly, we plot P_k against \bar{i}_k in Figure 6(a). Here we see qualitatively similar results to that of m_k . We also plot the mean \bar{P} of the participation number values P_k for each value of Δ in Figure 6(b), with error bars indicating one SD from \bar{P} . Clearly, both the spread and mean of each set of P_k values increase as Δ decreases.

What we can conclude from these results is that normal mode distributions (on average) involve more lattice sites and are spread over larger regions of the lattice as we decrease Δ and approach an ordered LKG lattice. Since any excitation of the lattice is built from a linear combination of normal modes, this would suggest that the number of normal modes used to describe a single-site excitation of the lattice increases as we approach an ordered system.

For a single-site excitation of a (nonlinear) KG lattice, these results suggest that energy diffuses through such a lattice at a greater rate for smaller Δ values, since in the linear system such an excitation involves many poorly localised normal modes. In the next section we will study the diffusion of energy in nonlinear KG lattices.

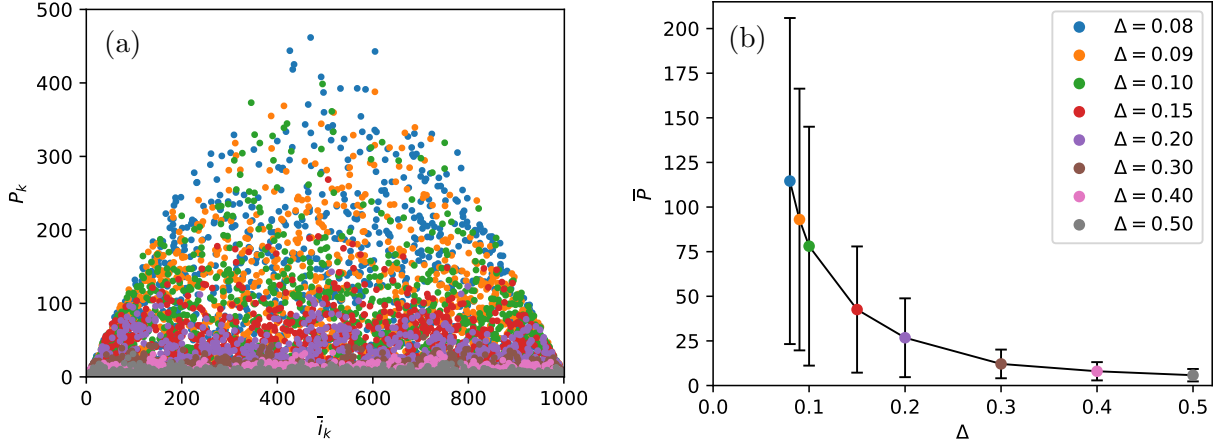


Figure 6: (a) Plot of participation number P_k of normal mode distribution v_{ki}^2 against the distribution mean \bar{i}_k , where each colour represents a value of Δ given in the legend of (b). (b) Plot of mean participation number \bar{P} against disorder radius Δ . Error bars indicate one SD from \bar{P} .

5 Nonlinear System: Wave Packet Evolution

5.1 Lattice Sizes

In order to simulate the diffusion of energy through an infinite KG lattice, we chose the lattice size N in our computations to be large enough so that the energy at the tails (i.e. lattice sites near the boundaries) was negligibly small. The energy at the tails, E_T , was computed by calculating the energy distribution ξ_i at the first 5 sites and the last 5 sites of the lattice chain, and then taking the mean of those values. In each computation, the lattice size was chosen to be as small as possible while ensuring that $E_T < 10^{-12}$ for the duration of the computation.

For each value of Δ used in our computations, we give the precise lattice size used in Table 1. We also give a plot of this relationship in Figure 7 together with the power law $N = 130\Delta^{-1.9}$ fitted to the plotted points. From this it is clear that as we approach an ordered system of $\Delta = 0$, the required lattice size for our computations diverges. As we will see, this is a result of energy spreading to the tails of the lattice faster as Δ decreases. Since the computation time scales with the lattice size of the system, using smaller values of Δ would require significantly more CPU time.

Δ	0.08	0.09	0.1	0.15	0.2	0.3	0.4	0.5
N	16001	12501	10001	4701	2801	1201	701	501

Table 1: Lattice size N required for each value of the disorder radius Δ .

5.2 Parameters and Initial Conditions

With the aim of building on the research of [7], we performed computations with the disorder strength set to $W = 4$ for a single-site excitation of the KG lattice with total energy $H = 0.4$, since these were the values used in that paper (in particular for the weak chaos regime). Unlike in the paper, however, we performed computations for multiple disorder parameters, namely $\Delta \in \{0.08, 0.09, 0.1, 0.15, 0.2, 0.3, 0.4, 0.5\}$. For each disorder realisation, the disorder parameters ϵ_i corresponding to each site were sampled uniformly at random from the interval $[1 - \Delta, 1 + \Delta]$.

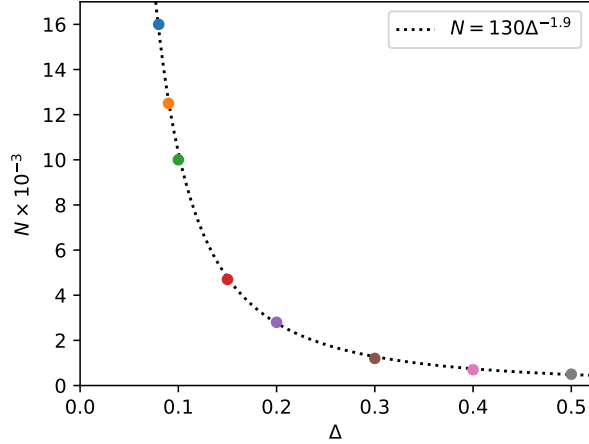


Figure 7: Plot of required lattice size N against disorder radius Δ . The dotted line is a fit of the power law $N = 130\Delta^{-1.9}$ to the plotted points.

However, we made an exception for the middle site of the lattice (the only site to be given energy initially), which we always gave a disorder parameter value of precisely 1 to ensure the initial behaviour of the middle site was consistent across disorder realisations.

We now address the method used to initiate a single-site excitation in the KG lattice. The energy of $H = 0.4$ was given to the middle site of the lattice in the form of kinetic energy, i.e. the initial displacement of the middle site was set to zero, while its initial momentum was set to $\pm\sqrt{2H}$. The sign of the momentum (which determines the direction of motion) was chosen randomly in each case. All other sites were initiated with zero displacement and momentum.

The deviations $\delta\vec{q}$ and $\delta\vec{p}$ were initialised by choosing the components of these vectors uniformly at random from the interval $[-1, 1]$. However, these components were only chosen for sites near the middle of the lattice, in particular the 11 central sites of the lattice centred on the middle site. All other components of the deviation vectors were initialised to zero. After this, each vector $\delta\vec{q}$ and $\delta\vec{p}$ was independently normalised.

In each case, we performed computations up to 10^7 time units. A time step of $\tau = 0.5$ was used throughout, as this was found to bound the absolute relative energy error E_r by approximately 10^{-5} , which is usually deemed an acceptable level of accuracy in such computations [8]. To show that E_r is indeed bounded appropriately, in Figure 8 we give a plot of E_r over time using $\tau = 0.5$ for a single disorder realisation of each of the extreme cases of disorder radius: $\Delta = 0.08$ and $\Delta = 0.5$.

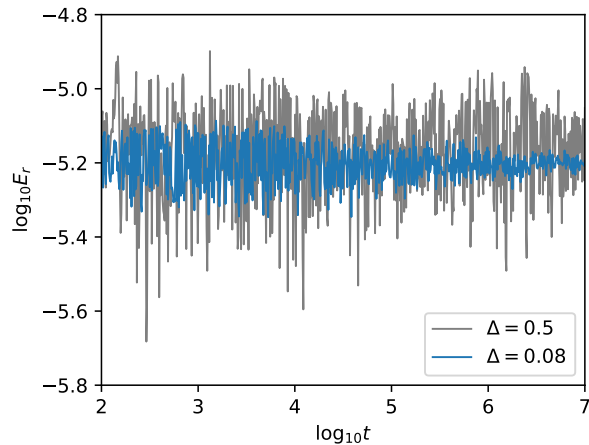


Figure 8: Plot of absolute relative energy error E_r against time t (in log-log scale) for a single disorder realisation with each of $\Delta = 0.08$ (in blue) and $\Delta = 0.5$ (in grey).

5.3 Profile of Energy Distribution and DVD

We can visualise the spreading of a wave packet of energy through the KG lattice over time by plotting the energy distribution ξ_i at various points in time during the computation. This is done in Figure 9(a) for a random disorder realisation with disorder radius $\Delta = 0.5$ (all other parameters and initial conditions are given in Section 5.2). In this case, the lattice size is $N = 501$, with the middle site at $i = 251$. From this it is clear that the energy distribution continually spreads through the lattice until the final time computed of 10^7 units, which is in agreement with comparable results given in [7] for $\Delta = 0.5$. This is in contrast to the LKG model which has the property of Anderson localisation [21] which prevents the energy distribution from delocalising further after some time. From Figure 9(a), it appears that Anderson localisation does not occur in the nonlinear KG model (within the time limit of our computation).

The evolution of the DVD over time (for the same disorder realisation) may also be visualised in a similar way. This is given in Figure 9(b). We see from the figure that the DVD barely spreads between times 10^3 and 10^7 , maintaining a pointy triangular profile. This persistent localisation of the DVD is in agreement with results presented in [7][11].

These results are expanded on in Section 5.4 where we study the second moment and participation number corresponding to these distributions.

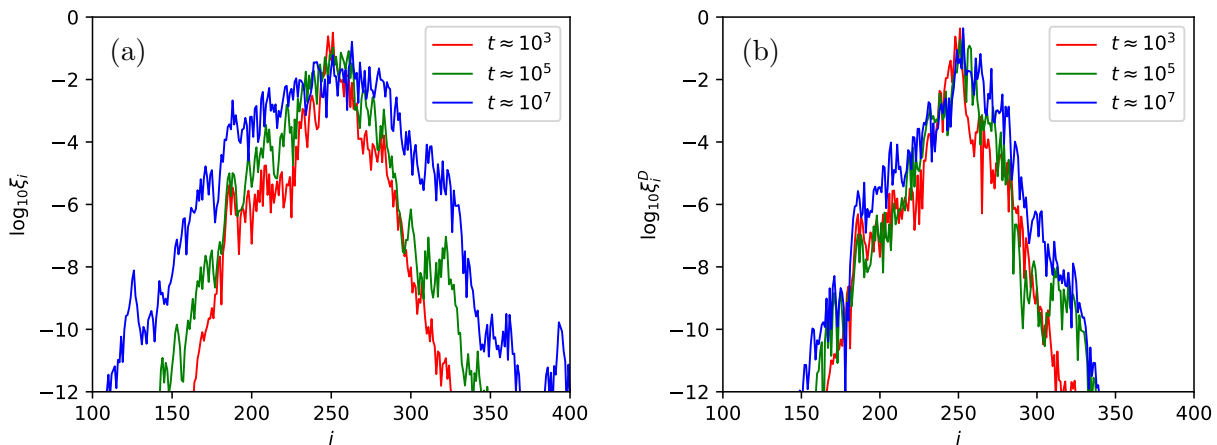


Figure 9: Plot of (a) energy distribution ξ_i and (b) DVD ξ_i^D (each in log scale) against the lattice sites i for a random disorder realisation of a single-site excitation with $\Delta = 0.5$. In both figures, a plot is given for each of the times $t \approx 10^3$ (in red), $t \approx 10^5$ (in green), and $t \approx 10^7$ (in blue).

5.4 Diffusion and Chaoticity Results

Using the parameters and initial conditions from Section 5.2, we performed computations for 20 random disorder realisations of the KG lattice with each value of Δ . By repeating computations for many disorder realisations, our results could be averaged to yield more accurate estimates from the data. We note, however, that a few disorder realisations invariably yielded misbehaving results, where the values of m , P , or Λ evolved significantly differently to the corresponding average. Such misbehaving realisations were removed from our sample and replaced with realisations which behaved.

Consider now the second moment m_j computed using the j^{th} disorder realisation. By taking the mean of these values m_j across realisations, we produce a better estimate of the second moment,

which we call $\langle m \rangle$. Now, since we will be presenting the results in log-log scale, the quantity we are interested in is actually $\log_{10}\langle m \rangle$. However, in order to determine the rate of change of $\log_{10}\langle m \rangle$ in log scale, we will need to differentiate it with respect to log time, $\log_{10} t$. This is an issue, since such computational results are generally not smooth enough to be directly differentiated numerically. Therefore, we first smooth the $\log_{10}\langle m \rangle$ curve over time using a LOWESS smoothing algorithm [22]. We call this smoothed curve $\langle \log_{10}\langle m \rangle \rangle$, and we plot it against time in Figure 10(a). Following exactly same procedure for the participation number P , we plot the smoothed logarithm of the mean participation number $\langle \log_{10}\langle P \rangle \rangle$ in Figure 10(b).

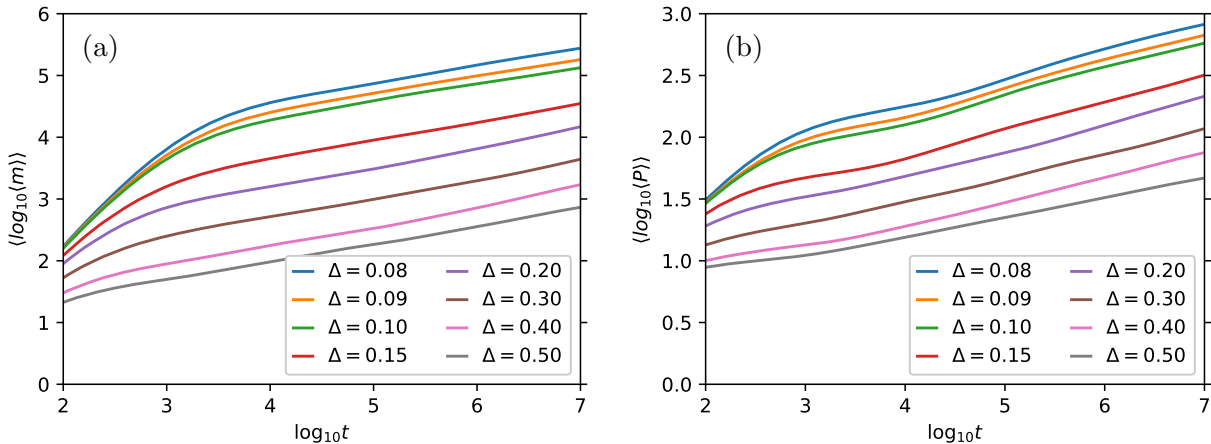


Figure 10: Plots of the smoothed logarithm of (a) mean second moment $\langle m \rangle$ and (b) mean participation number $\langle P \rangle$ against log time $\log_{10} t$ for each disorder radius value Δ .

In order to describe the slopes of each curve in Figure 10, we define the slope of the quantity A in log-log scale as follows [7]:

$$\alpha_A = \frac{d\langle \log_{10}\langle A \rangle \rangle}{d(\log_{10} t)}, \quad (22)$$

where A is the quantity of interest (m or P , in this case). Since the slope of each curve in the figure appears to tend to a constant, it follows that the evolution of m and P over long periods of time are governed by the power laws $m \propto t^{\alpha_m}$ and $P \propto t^{\alpha_P}$. We will soon discuss how α_m and α_P vary with respect to Δ , but for now we simply note that from Figure 10 alone it appears that the slopes α_m and α_P do not vary significantly with respect to Δ . Now we see from these figures for m and P that as Δ decreases, the curves are shifted upwards in the respective plots. As the plots are in log-log scale, this upward translation corresponds to an increase in the proportionality factor of the power laws given for m and P . Therefore, we see that both m and P grow at faster rates over the time period computed when Δ is decreased. In other words, energy diffuses faster in more ordered KLG lattices. These results agree with our prediction in Section 4 from our analysis of the normal modes of LKG lattices.

Upon closer inspection of Figure 10, however, it is clear that there is some small variation between slopes with different disorder radii. To see this, we plot α_m and α_P over time for each Δ in Figures 11(a) and (b), respectively. From the plots, it is clear that both α_m and α_P have different values near the final time 10^7 for each Δ . To determine this relationship, we first estimate a final value for these quantities. Instead of simply taking the value at the final time 10^7 , we take the mean of each of α_m and α_P over the interval $[10^{6.5}, 10^7]$. We plot these end-averaged values of α_m and α_P

against Δ in Figure 12. These results suggest that both α_m and α_P increase initially as Δ decreases from 0.5, but then decrease again as Δ approaches 0.1. However, such a relationship would imply that, over very long times, energy diffuses through a more ordered KG lattice of $\Delta \approx 0.1$ more slowly than in slightly less ordered lattices of $\Delta \approx 0.3$, contrary to our expectations from the LKG normal mode analysis. Nevertheless, without a clearer trend, the long-term relationship between each slope and Δ is inconclusive.

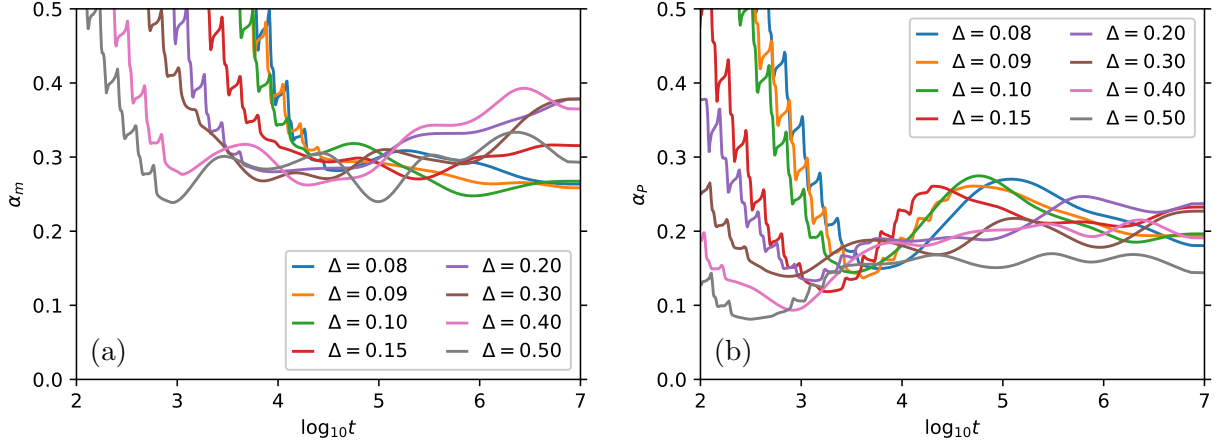


Figure 11: Plots of the slope (a) α_m for the second moment and (b) α_P for the participation number over log time $\log_{10} t$ for each disorder radius value Δ .

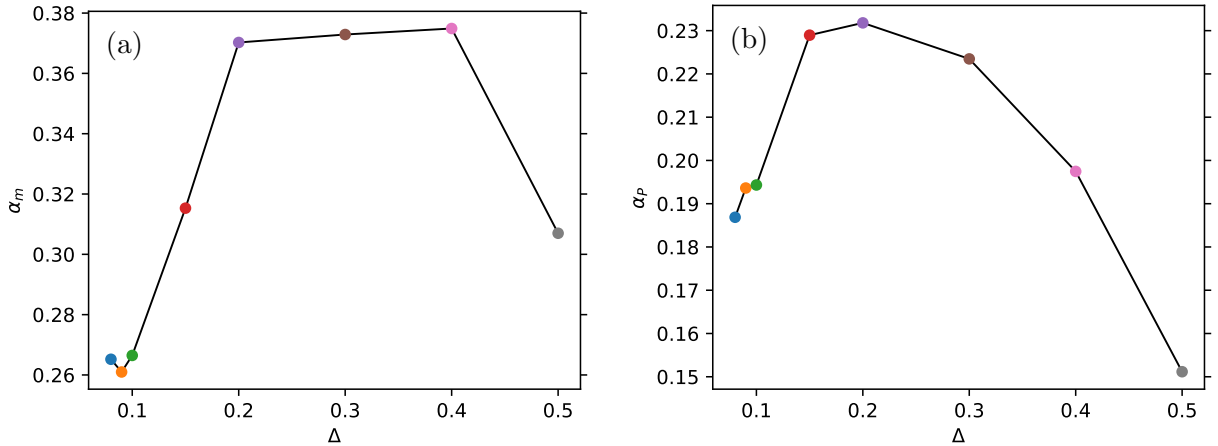


Figure 12: Plots of the end-averaged slope (a) α_m for the second moment and (b) α_P for the participation number against the disorder radius Δ . Black lines are only for guiding the eye.

We now turn to the DVD second moment m^D and DVD participation number P^D . Computing the relevant quantities for m^D and P^D in the same manner as done for m and P , we give completely analogous plots in Figures 13, 14 and 15. Again we find that, due to the vertical shifts in the curves of Figure 13, both m^D and P^D grow at faster rates as Δ decreases, indicating faster spreading of the DVD. However, we see from Figure 14 that the slope α_P^D is very near zero and α_m^D is also small, which suggests a very slow diffusion of the DVD through the KG lattice in each of these cases. This result agrees with what we observed in Section 5.3 and with comparable findings in [7]. However, the relationship between each of the end-averaged slopes and Δ in Figure 15 is inconclusive.

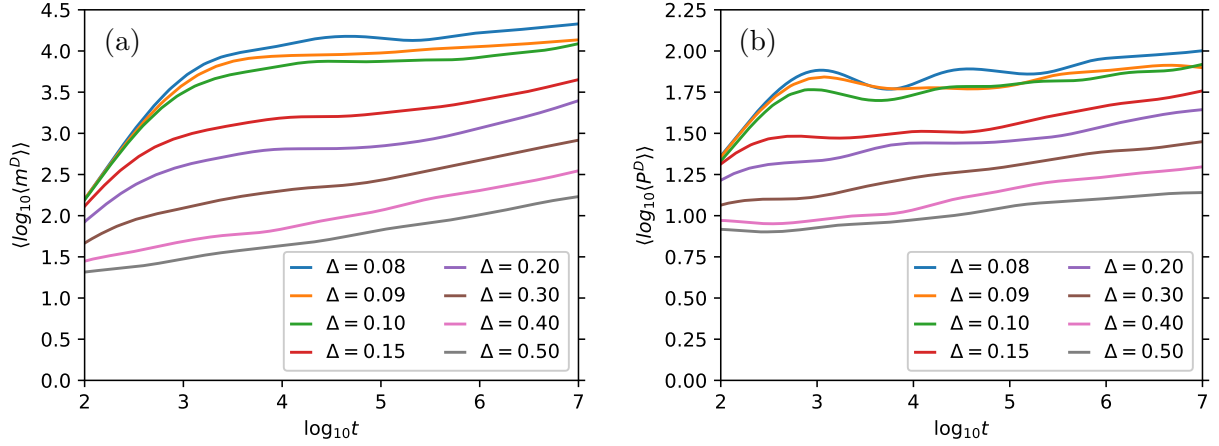


Figure 13: Plots of the smoothed logarithm of (a) mean DVD second moment $\langle m^D \rangle$ and (b) mean DVD participation number $\langle P^D \rangle$ against log time $\log_{10} t$ for each disorder radius value Δ .

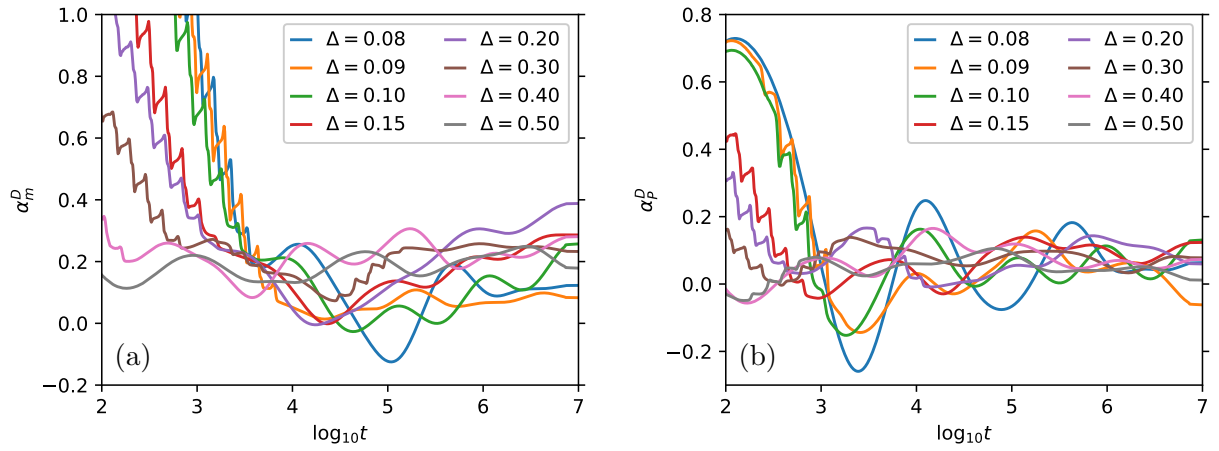


Figure 14: Plots of the slope (a) α_m^D for the DVD second moment and (b) α_P^D for the DVD participation number over log time $\log_{10} t$ for each disorder radius value Δ .

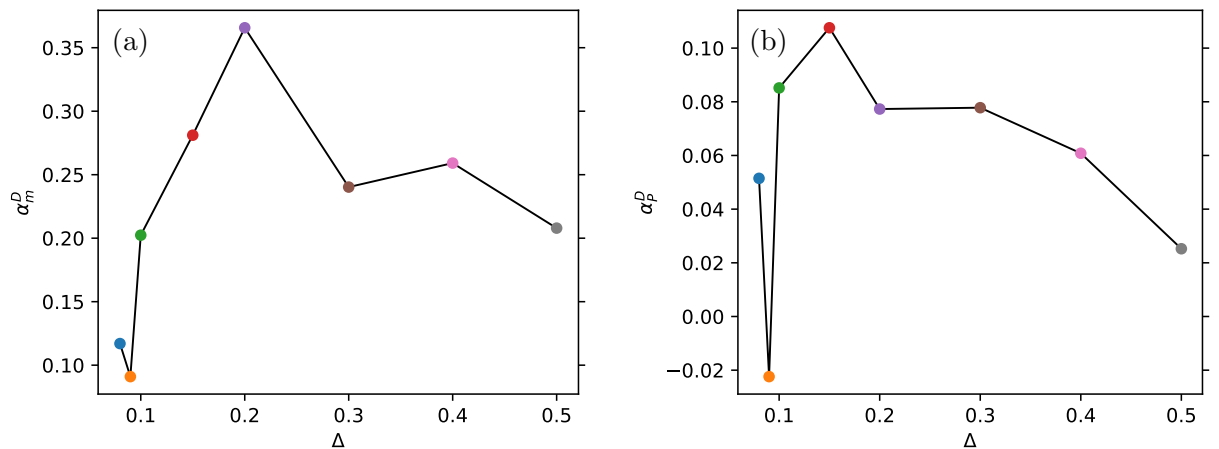


Figure 15: Plots of the end-averaged slope (a) α_m^D for the DVD second moment and (b) α_P^D for the DVD participation number against disorder radius Δ . Black lines are only for guiding the eye.

Performing the same analysis on the finite time MLE $\Lambda(t)$, we produce analogous plots in Figures 16 and 17. In this case, the relationship between the end-averaged slope α_Λ and Δ in Figure 17 indicates that α_Λ tends to increase with an increasing Δ . Therefore, it can be seen from the power law $\Lambda \propto t^{\alpha_\Lambda}$ that the finite time MLE decays faster for more ordered systems, suggesting that more ordered KG lattices are less chaotic.

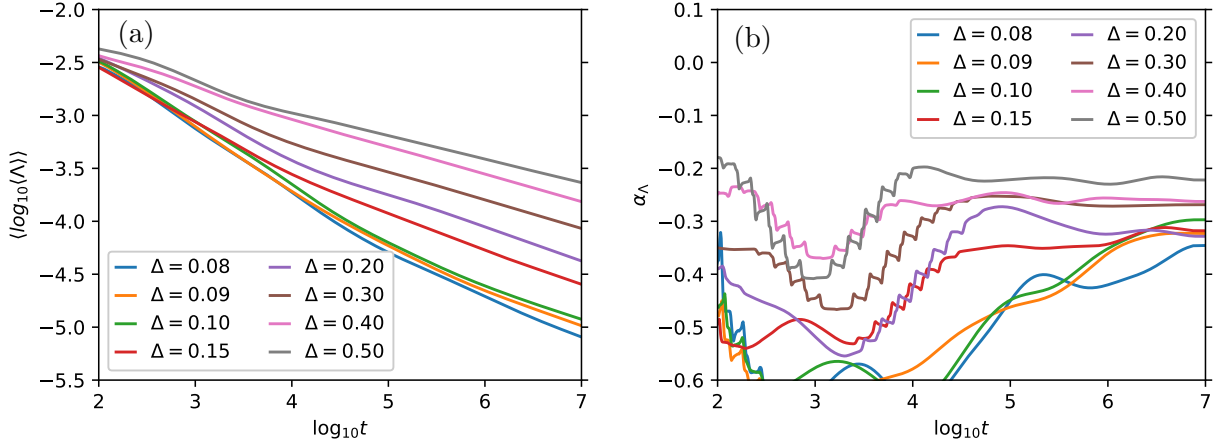


Figure 16: Plots of (a) the smoothed logarithm of the mean finite time MLE $\langle \Lambda \rangle$ and (b) the slope α_Λ over log time $\log_{10} t$ for each disorder radius value Δ .

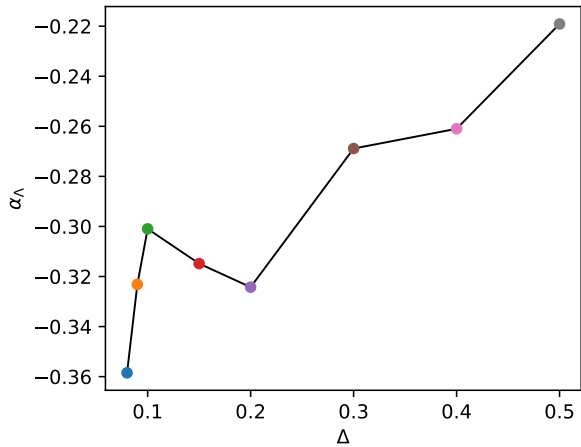


Figure 17: Plot of the end-averaged slope α_Λ for the finite time MLE against the disorder radius Δ . Black lines are only for guiding the eye.

For $\Delta = 0.5$, it was determined in [7] using computations up to 10^8 that $\alpha_m \approx 1/3$, $\alpha_P \approx 1/6$, and $\alpha_\Lambda \approx -1/4$. In comparison, our computations up to 10^7 with $\Delta = 0.5$ for the end-averaged slopes yielded the following estimates (to two significant figures): $\alpha_m \approx 0.31$, $\alpha_P \approx 0.15$, and $\alpha_\Lambda \approx -0.22$. While there is some small discrepancy between these values, our results for these quantities appear to agree with the published results.

6 Discussion and Conclusion

Through analysing the normal modes of the LKG model in Section 4, we uncovered various properties of the normal mode distributions. In particular, it was determined that decreasing the disorder radius Δ resulted in an increase of the mean second moment and mean participation number of

these distributions. As a result, it was predicted that for energy diffusing through a (nonlinear) KG lattice, the second moment and participation number of the wave packet would also increase as we approach an ordered lattice.

In Section 5, we excited a single site of the KG lattice for various values of Δ and evolved the system until a final time of 10^7 units. In the case of $\Delta = 0.5$, similar results to [7] were obtained for the power laws governing m , P , and Λ evolution, with minor differences. It was also found that when decreasing Δ , the rate of change of both m and P increased as expected while maintaining a similar power law for each Δ . Upon closer inspection, however, the slopes α_m and α_P were found to be dependent on Δ . Though these relationships could not be conclusively determined, this result warrants further investigation, particularly using longer computations of at least 10^8 .

The DVD was found to remain somewhat localised over the computed time period of 10^7 . In particular, the participation number of the DVD was found to remain practically constant over time, suggesting that the number of lattice sites involved in deviations does not increase significantly over time. The second moment was found to increase over time, though very slowly. This agrees with similar findings in [7].

As for the effect of disorder on chaoticity, the slope α_Λ for the finite time MLE was found to decrease overall when decreasing Δ . This suggests that more ordered lattices are less chaotic than less ordered lattices. A possible mechanism for this is as follows: since $\Lambda(t)$ decreases as energy diffuses through the lattice, the faster rate of decay of $\Lambda(t)$ may be a result of the increased growth rates of m and P for small disorder radii.

References

- [1] A. A. Ovchinnikov, N. S. Erikhman, and K. A. Pronin. *Vibrational-Rotational Excitations in Nonlinear Molecular Systems*. Springer US, 2001.
- [2] L. Proville. Dynamical structure factor of a nonlinear Klein-Gordon lattice. *Physical Review B*, 72:184301, 2005.
- [3] Ch. Skokos. *The Lyapunov Characteristic Exponents and Their Computation*, volume 790 of *Lecture Notes in Physics*, pages 63–135. Springer-Verlag Berlin Heidelberg, 2010.
- [4] R. Shankar. *Principles of Quantum Mechanics*. Springer US, 2nd edition, 1994.
- [5] R. L. Devaney. *An Introduction to Chaotic Dynamical Systems*. Addison-Wesley advanced book program. Addison-Wesley, 1989.
- [6] J. Banks, J. Brooks, G. Cairns, G. Davis, and P. Stacey. On Devaney’s Definition of Chaos. *The American Mathematical Monthly*, 99(4):332–334, 1992.
- [7] B. Senyange, B. Many Manda, and Ch. Skokos. Characteristics of chaos evolution in one-dimensional disordered nonlinear lattices. *Physical Review E*, 98:052229, 2018.
- [8] B. Senyange and Ch. Skokos. Computational efficiency of symplectic integration schemes: application to multidimensional disordered Klein–Gordon lattices. *The European Physical Journal Special Topics*, 227(5):625–643, 2018.
- [9] S. Flach, D. O. Krimer, and Ch. Skokos. Universal Spreading of Wave Packets in Disordered Nonlinear Systems. *Physical Review Letters*, 102:024101, 2009.

- [10] Ch. Skokos, D. O. Krimer, S. Komineas, and S. Flach. Delocalization of wave packets in disordered nonlinear chains. *Physical Review E*, 79:056211, 2009.
- [11] Ch. Skokos, I. Gkolias, and S. Flach. Nonequilibrium Chaos of Disordered Nonlinear Waves. *Physical Review Letters*, 111:064101, 2013.
- [12] V. I. Arnol'd. *Mathematical Methods of Classical Mechanics*. Graduate Texts in Mathematics. Springer-Verlag New York, 2nd edition, 1997. Translated by A. Weinstein and K. Vogtmann.
- [13] R. L. Burden and J. D. Faires. *Numerical Analysis*. Cengage Learning, 9th edition, 2011.
- [14] D. Donnelly and E. Rogers. Symplectic integrators: An introduction. *American Journal of Physics*, 73(10):938–945, 2005.
- [15] S. Blanes, F. Casas, A. Farrés, J. Laskar, J. Makazaga, and A. Murua. New families of symplectic splitting methods for numerical integration in dynamical astronomy. *Applied Numerical Mathematics*, 68:58–72, 2013.
- [16] Ch. Skokos and E. Gerlach. Numerical integration of variational equations. *Physical Review E*, 82:036704, 2010.
- [17] Python. <https://www.python.org>.
- [18] NumPy. <https://www.numpy.org>.
- [19] Numba: A High Performance Python Compiler. <https://numba.pydata.org>.
- [20] SciPy v1.3.0 Reference Guide. https://docs.scipy.org/doc/scipy/reference/generated/scipy.linalg.eigh_tridiagonal.html.
- [21] P. W. Anderson. Absence of Diffusion in Certain Random Lattices. *Physical Review*, 109:1492–1505, 1958.
- [22] StatsModels v0.10.1 Documentation. https://www.statsmodels.org/stable/generated/statsmodels.nonparametric.smoothers_lowess.lowess.html.